Desalination 583 (2024) 117674

Contents lists available at ScienceDirect

Desalination

journal homepage: www.elsevier.com/locate/desal

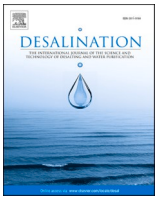

Redox-mediated ion separation and exchange by tailored design of immobilized metallopolymers

Deborah Schmitt [a], Markus Gallei [a,b,*]

[a] Polymer Chemistry, Saarland University, Campus C4 2, 66123 Saarbrücken, Germany
[b] Saarene, Saarland Center for Energy Materials and Sustainability, Campus C4 2, 66123 Saarbrücken, Germany

HIGHLIGHTS

- Anionic (block) copolymerization of redox-active monomers from the surface of organic microparticles is described.
- Reversible redox-switchable and electrochemically mediated ion sorption and exchange are shown.
- Polarity of the comonomer shows an impact on ion sorption capacity within flow-through experiments

GRAPHICAL ABSTRACT

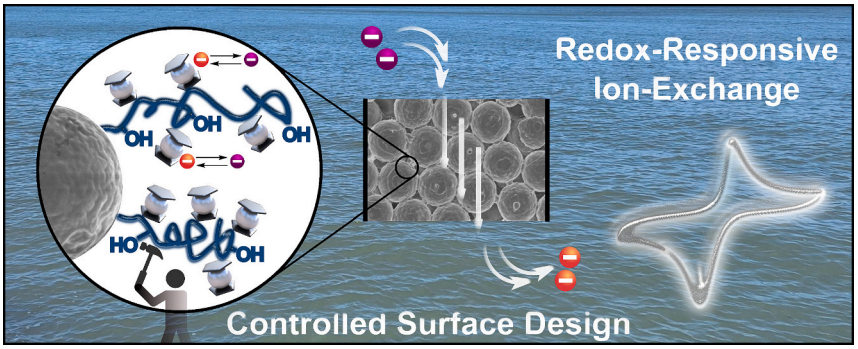

ARTICLE INFO

Keywords:
Porous particles
Metallopolymers
Surface functionalization
Anionic polymerization
Ion exchange
Flow experiments
Block copolymers

ABSTRACT

Mining and harvesting of valuable components from water or organic phases are urgent challenges. Metallopolymers can show excellent control of the binding and release of target molecules or ions without additional external chemical inputs. Here, we report the covalent functionalization of porous polystyrene microparticles with poly(hydroxyethyl methacrylate) (PHEMA) and poly(ferrocenylmethyl methacrylate) (PFMMA) copolymers and block copolymers via surface-initiated living anionic polymerization to tailor the functionality and polarity of the surface. The metallopolymer-decorated particles were characterized by infrared spectroscopy, scanning electron microscopy, and energy-dispersive X-ray spectroscopy, and the redox-responsiveness was analyzed in different media using cyclic voltammetry. The variation in polarity enabled the investigation of the influence of polarity on the electrochemical performance. The metallopolymer particles were used as efficient ion-adsorbers and ion-exchange materials in both static and flow measurements, and the resulting findings were compared to homopolymer-functionalized particles. The adsorption of fluoride, nitrate, and sulfate and their adsorption selectivity were investigated. The capacity of sulfate was increased for hydrophilic particles and remained more constant over time. The results demonstrate the importance of the controlled design of surfaces for tailoring the efficiency of ion-adsorption materials. The insights on the structure-property relation of the metallopolymer immobilization pave the way for new adsorption technologies and future design of electrochemically switchable surfaces.

* Corresponding author at: Polymer Chemistry, Saarland University, Campus C4 2, 66123 Saarbrücken, Germany.
E-mail address: markus.gallei@uni-saarland.de (M. Gallei).

https://doi.org/10.1016/j.desal.2024.117674
Received 18 March 2024; Received in revised form 21 April 2024; Accepted 21 April 2024
Available online 1 May 2024

1. Introduction

Ion exchange materials are omnipresent in everyday life and play a crucial role in society in the field of water purification [1,2], water analysis [3], or water filtration [4]. A few of the oldest applications of ion exchange resins are the removal of pollutants, reducing high ion concentrations in water, or softening of water [5,6]. These materials are of great importance in agriculture, for example, as nitrate or sulfate accumulates in high concentrations [7,8]. While sulfate in low concentrations plays an important role for humans and the environment, excessive concentrations lead to health risks or corrosion issues [9–11]. Climate change, which favors the accumulation of high concentrations of sulfate in water, strongly increases these issues [12,13]. Ion exchange resins can be used to overcome these challenges. These materials are based on a structural component which is often composed of a highly porous polymer matrix such as cross-linked polystyrene particles. As a second compound, ion exchange resins contain functional ionic groups, mostly amines, that enable the ion exchange process [14,15]. Using such resins for softening of water, removal of pollutants from water, or general analysis of water results in an ion exchange of the initially present counter ions with the ions to be adsorbed or analyzed. The equilibrium of the reversible process is dependent on the affinity of the ions to the functional groups of the resin and the ion concentration. By rinsing the resins with a highly concentrated ionic solution containing the initial counter ions, a regeneration of the exchangers can be achieved by shifting the equilibrium, which facilitates a renewed ion exchange process [16,17]. However, the demands placed on modern separation systems are extremely high, not least due to the immense challenges posed by today's separation problems. For this reason, many researchers are engaged in the optimization and improvement of such materials or the development of new material classes for ion exchange applications. One strategy for addressing this issue can be to hydrophilize the materials [18], as hydroxyl groups can support the elution of the ions to be analyzed through the hindrance of non-ionic interactions [19–22]. Zatirakha et al. functionalized micrometer-sized polystyrene particles with amine-containing functional groups and hydroxylated the particles by introducing OH groups to apply them as ion exchangers in chromatographic systems. Compared to materials without OH groups, higher column performance and a better peak geometry could be generated [23]. In addition, Yang et al. were able to significantly reduce analysis times by introducing hydroxy groups [24].

Recently, stimuli-responsive polymers have attracted attention for the development of innovative ion exchange systems. Stimuli-responsive materials can change properties by applying external stimuli like temperature [25], pH value [26], light [27], mechanical stress [28], redox agents, or an electrical field [29–31]. The most studied materials are temperature or pH-based [32–35], but systems that provide a fast switchability due to non-diffusion limitations such as light or redox-responsiveness are also of significant interest. Metallopolymer-based functionalizations represent a fascinating class of stimuli-responsive polymers here. These metallopolymer-based, mostly ferrocene-containing, surfaces can change properties by applying redox reagents or an electric potential to switch between the neutral, hydrophobic ferrocene to the positively charged, hydrophilic ferrocenium [36–38]. As a result, the neutral polymer can be converted into a positively charged ferrocenium polyelectrolyte and thus, the polymer brush structure is affected at the surface [39,40]. These changes in capabilities enable applications in catalysis [41,42], separation processes [43–45], or sensing materials [46]. Therefore, ferrocene-containing materials play a crucial role in the field of electrochemistry. For example, ferrocene-containing particles can be utilized to prepare redox-responsive opal films, which can be investigated among their electrochemical responsiveness [47–49]. The systematic design of ferrocene-containing polymer interfaces on the molecular level is thereby a key factor for the applications and enables new-generation materials with enhanced properties [50,51]. For instance, Jeon et al. developed an electrochemical sensing electrode by using a polymer with chiral ferrocene units and could therefore enhance the recognition of enantiomeric target molecules [52]. Su et al. were able to capture arsenic and chromium oxyanions from water with high selectivities [44]. The controlled design of ferrocene polymers with different electronic situations directly next to the ferrocene group could prove a remarkable avenue to tailor the selectivity of the polymers by PFAS capture [53]. Furthermore, the incorporation of non-redox-active, hydrophilic co-monomers in ferrocene-containing polymer-based materials facilitates the overcoming of hydrophobicity issues [54], which resulted in a significant increase in selectivity in electrochemical-driven ion-adsorption processes [55,56]. However, avoiding leaching of the polymers is a major challenge in the application of electrochemical devices and this issue is even more prominent in hydrophilized polymers, that are often applied in polar solvents [57]. For this reason, the covalent immobilization of the polymers on surfaces offers an increased relevance for redox-responsive materials [58–61].

The most common preparation method for immobilized polymer brushes represents the grafting-from polymerization, in which the initiator is provided through covalent bonding to the surface. The polymerization emerges directly from the surfaces and offers the possibility of high polymer capacities [62–64]. Mazurowski et al. used the grafting-from method to synthesize poly(2-(methacryloyloxy)ethyl ferrocenecarboxylate) polymer brushes via surface-initiated atom transfer radical polymerization (SI-ATRP) for investigation of the swelling capabilities of resulted particles [40]. In addition, the preparation of poly (ferrocenylmethyl methacrylate) (PFMMA) brushes on glassy carbon surfaces was realized to investigate the electron transfer process in the polymer coating [65]. However, especially in electrochemical applications of metallopolymers, metal impurities from the ATRP catalyst can affect the results of separation processes [66,67]. For this reason, living anionic polymerization on surfaces represents a facility for anchoring specifically designed polymer brushes on surfaces without the addition of harmful impurities. Because of the high purity requirements of the substrates and the reagents, this method has been less studied on surfaces. Jordan et al. described the surface-initiated living anionic polymerization (SI-LAP) of styrene on gold substrates in 1999. The Advincula group utilized this technique on silica substrates for the polymerization of polystyrene homopolymers [68–70] and block copolymers of styrene and isoprene [71]. The polymerization of ethylene oxide and methyl methacrylate (MMA) has been described, too, but high degrees of functionalization have not been realized [72–74]. In addition, stimuli-responsive polymers have been anchored on polystyrene nanoparticles by using ansa-ferrocenophane as a monomer [75]. Recently, we described the functionalization of polystyrene microparticles with MMA, 2-(trimethylsiloxy)ethyl methacrylate (HEMA-TMS), FMMA, and vinyl ferrocene homopolymers [54,76]. The polymerization process was described in more detail and the degree of functionalization could be tailored up to high degrees of polymer coating (more than 50 %). However, to the best of our knowledge, no functional or redox-responsive copolymers or block copolymers have been polymerized on surfaces using SI-LAP.

In the present study, we report the SI-LAP as a powerful method for tailored surface functionalization with copolymers and block copolymers. For this SI-LAP approach, we used porous polystyrene microparticles as substrate and HEMA-TMS as well as the redox-responsive FMMA as monomers. Various degrees of hydrophilization were explored by using different HEMA(-TMS) contents. The functionalization of resulting particles was confirmed through attenuated total reflection infrared (ATR-IR) spectroscopy and the homogeneity of the coating was analyzed using scanning electron microscopy (SEM) and energy-dispersive X-ray spectroscopy (EDS). Furthermore, the electrochemical addressability of the functionalized particles was studied by cyclic voltammetry in different media, and the influence of polarity on electrochemical behavior was investigated by using the TMS-protected block copolymer-functionalized particles and their deprotected pendants. In

addition, the application of the particles as ion adsorption and ion exchange materials was examined by static and flow experiments based on chemical oxidation and reduction, or flow-through regeneration processes. For this study, the homopolymer-functionalized particles were utilized as comparing material. The influence of the hydrophilization on the selectivity or the rate of the ion exchange process was examined both, with and without competition of inorganic anions.

2. Experimental section/methods

2.1. Materials and instrumentation

All reagents and solvents were purchased from Fisher Scientific, TCI Chemicals, Sigma Aldrich, or Alfa Aesar and, if not otherwise specified, used as received. Polystyrene-divinylbenzene particles (PSDVB, 55 wt% DVB in ethyl vinyl benzene) were donated by Metrohm AG and dried for polymerization by repeated distillation in THF as described previously [76]. High-purity multi-walled carbon nanotubes (MWCNTs, NC7100) were provided from Nanocyl. Phenol was freshly sublimed. THF was dried with *n*-butyl lithium (*n*-BuLi, 1.6 M in *n*-hexane) and freshly distilled before use. Lithium chloride, diphenylethylene, methanol, HEMA-TMS, and FMMA were purified and dried as previously described. PFMMA, PHEMA-TMS, and PHEMA homopolymers as well as FMMA monomer were synthesized as described previously [76]. All syntheses were carried out under an inert gas atmosphere. All chemicals for adsorption measurements were purchased from Supelco and possess the purity grade for analysis EMSURE.

The anionic polymerizations were performed in A Braun Unilabplus Eco glovebox system equipped with a Julabo FP89 cryostat. NMR spectroscopy was performed with a Bruker AVANCE II 400 MHz spectrometer in $CDCl_3$ after filtration of the samples through a syringe filter to remove the particles. The spectra were referenced relative to the residual solvent signal [77] and evaluated with MestReNova. ATR-IR measurements were carried out on a Bruker Alpha II FT-IR spectrometer in transmittance. The evaluation and baseline correction was conducted with OPUS 8.5 and all spectra were normalized between 0 and 1. SEM images were collected on a Zeiss Sigma VP device (GeminiSEM 500) with an in-lens detector by using SmartSEM 6.07 as software. The images were recorded with an acceleration voltage of 3 kV in high current mode and an aperture of 20 μm. The samples were mounted on an aluminum stud using carbon tape, a copper grid, or a copper foil. All samples were sputter coated with ~6 nm platinum using an Automatic Turbo Coater Plasmatool 125 SIN 2020_131 from Ingenieurbüro Peter Liebscher. EDS spectra were collected with an SE2 detector using an acceleration voltage of 20 kV. Inductivity coupled plasma optical emission spectroscopy (ICP-OES) was performed for the elements iron and silicon with an ICP-OES Model Spectro Arcos after aqua regia digestion in a microwave in a CEM MARS 6 by MicroLab Kolbe in Oberhausen after drying for 24 h under 120 °C. CV was carried out on a Biologic SP-150 potentiostat and evaluated with EC-Lab V11.46. All measurements were calibrated with ferrocene. The adsorption experiments were carried out using a kdScientific KDS 100 legacy syringe pump with a flow rate of 3.5 mL min^{-1}. For ion chromatography, a 930 Compact IC Flex Ove/SeS/PP/Deg at 45 °C equipped with a 2 mL Dosino, the Metrohm intelligent Partial Loop Technique, and a conductivity detector were used. Aqueous 3.6 mmol L^{-1} Na_2CO_3 solution was used as mobile phase on a Metrosep Supp 7 250/2.0 column with a Metrosep RP 3 Guard HC/4.0 and a flow rate of 0.2 mL min^{-1}. The evaluation was accomplished with MagIC Net 3.3 software.

2.2. Synthesis of PSDVB@CP-1 via SI-LAP

200 mg PSDVB particles in a reaction flask equipped with a KPG stirrer were dispersed in 50 mL THF. The dispersion was cooled to -78 °C and titrated and activated with a total of 70 μL (91 μmol) *s*-butyl lithium (*s*-BuLi, 1.3 M in *n*-hexane). The orange particles were stirred for 30 min, warmed to room temperature, and stirred for 2 h. After adding 40 μL (227 μmol) diphenylethylene, a red particle dispersion was obtained and stirred for 15 min at room temperature. 75 mg (1.77 mmol) LiCl was added, and the mixture was cooled to −78 °C. The polymerization was started by quickly adding the monomer mixture of 500 mg (2.29 mmol) HEMA-TMS and 500 mg (1.76 mmol) FMMA in 4 mL THF. The reaction was terminated after 2 days with methanol and stirred for 30 min. The particles were cleaned by multiple centrifugation steps for 10 min at 2370 rcf, after redispersion in THF, toluene, distilled water, pyridine, and methanol, respectively. The particles were dried in a vacuum.

2.3. Exemplary synthesis of PSDVB@BCP-TMS-1 via SI-LAP

An amount of 150 mg PSDVB particles were dispersed in 50 mL THF in a reaction flask equipped with a KPG stirrer in a glovebox and cooled to −78 °C. The dispersion was titrated with a total amount of 70 μL (91 μmol) *s*-BuLi until a yellow-orange color was obtained. After stirring for 40 min, the mixture was warmed to room temperature and stirred for 2 h. 40 μL (227 μmol) diphenylethylene was added and stirred for 15 min. After adding 75 mg (1.77 mmol) LiCl, the dispersion was cooled to −78 °C and the polymerization was started by quickly adding 400 μL (1.83 mmol) HEMA-TMS. After 2.5 h, an aliquot of PSDVB@FB-1 particles was taken for IR and SEM analyses. A mixture of 250 μL HEMA-TMS (1.15 μmol) and 300 mg (1.06 μmol) FMMA in 2 mL THF was added for polymerization of the second block. The polymerization was terminated after 2 days by adding methanol, stirred for 30 min, and centrifugated. The particles were cleaned by multiple centrifugation steps for 10 min at 2370 rcf, after redispersion in THF, toluene, distilled water, pyridine, and methanol, respectively. The particles were dried in a vacuum. The experimental details of the other particle batches can be found in Table S1 (Supplementary Information).

2.4. Exemplary deprotection of PSDVB@BCP-TMS-1

50 mg PSDVB@BCP-TMS-1 were dispersed in 5 mL of a 0.1 M tetrabutylammonium fluoride (TBAF) solution in THF at 0 °C and stirred for 1 h. After stirring for 1 h, the dispersion was warmed to room temperature and stirred for further 18 h. The particles were centrifugated for 10 min at 2370 rcf and washed 5 times with saturated aqueous Na_2CO_3. For cleaning, the particles were redispersed in THF, methanol, pyridine, and diethyl ether, respectively. The particles were dried in a vacuum.

2.5. Electrochemical measurements

50 mg MWCNTs were dispersed in 10 mL ethanol by ultrasonic treatment for 30 min. 2 mg of the particles were swollen in ethanol, mixed with the MWCNT dispersion in a ratio 10/1, and 0.5 mg phenol was added. The dispersion was sonicated for 1 min and drop-coated on a glassy carbon working electrode (5 mm inner diameter) using two droplets. All measurements were performed with a three-electrode configuration by applying a scan rate of 20 mV s^{-1} using a Pt-wire as the counter electrode. The measurements in an aqueous solution were carried out with an Ag/AgCl reference electrode (equilibrated in 3 M NaCl) and $NaClO_4$ as electrolyte (0.1 M solutions). The measurements in acetonitrile (ACN) and chloroform were conducted with an $Ag/AgNO_3$ (ACN) or an Ag wire ($CHCl_3$) as a pseudo-reference electrode and tetrabutylammonium hexafluorophosphate as a supporting electrolyte (0.1 M solutions). Note, that phenol is not used during the preparation of PSDVB@BCP-TMS-1 for the measurement in chloroform due to an own signal in the increased measuring range.

2.6. Static ion adsorption measurements

2–3 mg functionalized particles were dispersed in 1 mL acetonitrile and allowed to swell for 1 h at room temperature. An excess of 20 mg (72 μmol) $FeCl_3 \cdot 6H_2O$ was added and allowed to be oxidized for 20 min.

The particles were centrifugated at 11180 rcf for 2 min and washed 10 times with acetonitrile via redispersion and centrifugation. The residue of the last washing cycle was analyzed for the removal of chloride content. The particles were dried under a nitrogen atmosphere and added to the stock solutions of 10 mg L^{-1} sulfate, 10 mg L^{-1} fluoride, 10 mg L^{-1} nitrate, or the multi-ion stock solution of 5 mg L^{-1} fluoride, 5 mg L^{-1} nitrate, and 4 mg L^{-1} sulfate, respectively. Sodium was used as a counterion in all cases. For time-dependent measurements, a sample was taken under a nitrogen atmosphere after 1, 10, 30, 60, and 120 min, respectively. For adsorption capacity determination and selectivity investigations, a sample was taken after 1 min. Solution concentrations were assessed using ion chromatography. All experiments were carried out twice.

2.7. Separation efficiency of static ion adsorption

(*i*) 2.99 mg and (*ii*) 5.27 mg oxidized, washed, and dried PSDVB@PFMMA particles were dispersed in 20 mL of an aqueous sulfate solution (5.37 mg L^{-1}), respectively. After 1 min, the particles were separated and the solution concentrations were assessed using ion chromatography. ($c_i(SO_4^{2-}) = 0.574$ mg L^{-1}; $c_{ii}(SO_4^{2-}) = 0.571$ mg L^{-1}).

2.8. Ion adsorption measurements in flow

2–4 mg functionalized particles were dispersed in 1 mL acetonitrile and allowed to swell at room temperature for 1 h. A syringe cannula (1.20 × 40 mm, 18 G × 1.5) was filled with glass wool and glass microfiber filter (1.6 µm pore size) first. The particle dispersion was added with a flow rate of 2 mL min^{-1}. A second layer of filter paper was inserted. The cannula was washed with 20 mL acetonitrile in flow. The flow rate during the experiment was set to 3.5 mL min^{-1}. The particles were oxidized with 10 mL $FeCl_3{\cdot}6H_2O$ solution in acetonitrile (0.1 M; 1 mmol), and washed with a mixture of 19.95 mL acetonitrile and 0.05 mL deionized water. The last 5 mL were analyzed regarding the removal of chloride content. Afterward, 5 mL of a stock solution containing 5 mg L^{-1} fluoride, 5 mg L^{-1} nitrate, and 4 mg L^{-1} sulfate were pumped through the cannula and analyzed (fraction 1). This process was repeated once for the cycle investigations (fraction 2) and four times for the time-dependent selectivity measurements (fraction 2–5). The particles were (*i*) reduced with 10 mL of a 0.1 M ascorbic acid solution (1 mmol) in (*i-1*) deionized water or (*i-2*) 1 M NaCl solution and afterward oxidized with 10 mL $FeCl_3{\cdot}6H_2O$ solution in acetonitrile (0.1 M; 1 mmol) for cyclic Red-Ox experiments or (*ii*) directly regenerated with 10 mL $FeCl_3{\cdot}6H_2O$ solution in acetonitrile (0.1 M; 1 mmol). This process was repeated four times. Solution concentrations of all samples were assessed twice using ion chromatography.

3. Results and discussion

3.1. Synthesis and characterization

The redox-responsive polymer brush was synthesized by surface-initiated living anionic polymerization (SI-LAP; Fig. 1). For this purpose, highly porous organic polystyrene microparticles (PSDVB), cross-linked with divinylbenzene, were used as substrate for functionalization. Two different kinds of polymer brushes were prepared as illustrated in Fig. 1a. On the one hand, 2-(trimethylsiloxy)ethyl methacrylate (HEMA-TMS) and ferrocenylmethyl methacrylate (FMMA) were statistically copolymerized. On the other hand, a block copolymer with PHEMA-TMS as the first block and PHEMA-TMS-*co*-PFMMA as the second block was grafted-from the particles. The first PHEMA block enabled the shielding of the hydrophobic PSDVB particles by forming a hydrophilic interlayer. The activation of PSDVB was carried out as described previously [76] with *s*-BuLi at −78 °C in THF followed by adding a sterically hindered group of diphenylethylene (DPE). The exclusion of non-immobilized initiator was carried out by the reaction of *s*-BuLi and THF forming different alcoholates [78–80].

To remove the protective TMS group, an excess of tetrabutylammonium fluoride was used resulting in more hydrophilic polymer brushes based on the hydroxyl group of PHEMA. Three different batches of the particles functionalized with block copolymers (PSDVB@BCP-TMS) were synthesized, varying the total amount of monomer and the ratio of

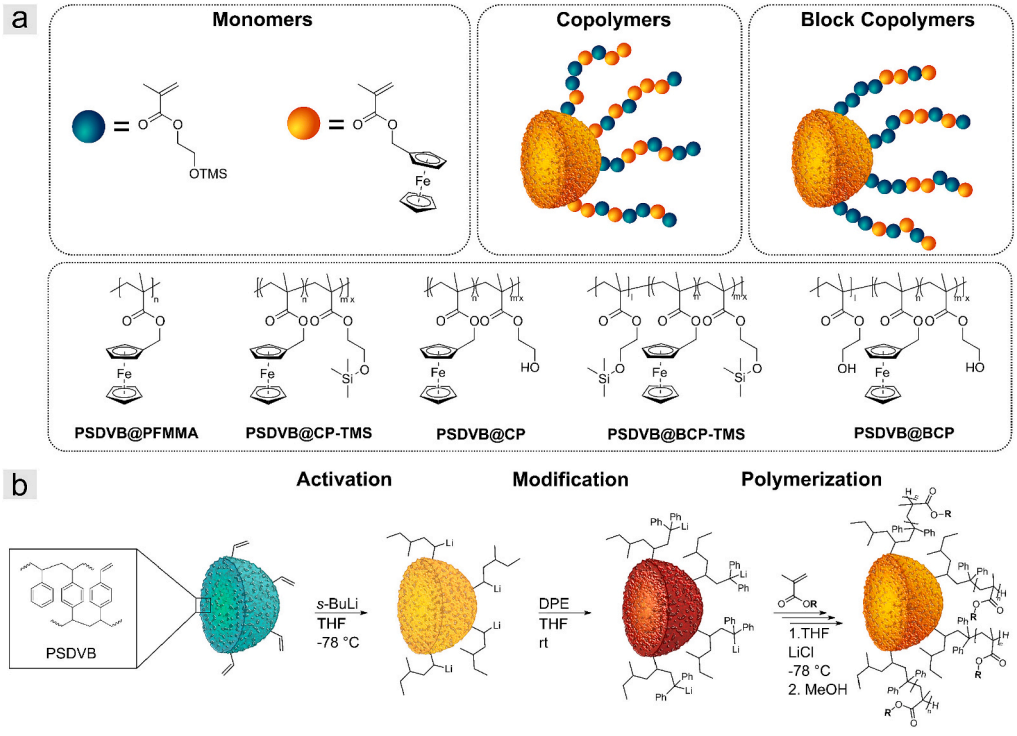

Fig. 1. a) Schematic illustration of grafted particles with copolymers or block copolymers in addition to the monomer structures of HEMA-TMS and FMMA and a summary of different polymer structures grafted from the particle surface. b) Stepwise grafting-from synthesis of methacrylates via one-pot SI-LAP reaction.

HEMA-TMS and FMMA monomers (Table S1). PSDVB@BCP-TMS-1 and PSDVB@BCP-TMS-2 contained equal amounts of HEMA-TMS in the first block. Whereas PSDVB@BCP-TMS-1 exhibited a similar ratio of both monomers in the second block during synthesis, in PSDVB@BCP-TMS-2 the amount of FMMA and thus the total amount of monomer was increased. It can be assumed that the reaction kinetics within the porous particles differ from free anionic polymerization in solution causing an incomplete conversion during the SI-LAP. This polymerization behavior of SI-LAP was demonstrated in a previous study for the homopolymers and is assumed to be the result of surface effects, side reactions, and the complex hierarchical porosity of the particles [76]. The conversion can generally be determined using ^{1}H NMR spectroscopy following the corresponding monomer concentrations. For example, in the case of PSDVB@FB-1 (particles with the first block of polymer functionalization only) the HEMA-TMS conversion was determined to be 40 % after 2 h. In PSDVB@BCP-TMS-3, the first block was synthesized to a higher degree compared to the second block due to a reduced amount of monomer. This assumption could be verified by inductively coupled plasma optical emission spectrometry (ICP-OES) measurement. For the calculation of the HEMA(-TMS) and FMMA contents, the Si and Fe content were used, respectively (Table S2). Besides the preparation of co- and block copolymers, the monomers could also be homopolymerized as described in a previous study [76], which can be realized on a 2.5–5 g scale.

ATR-IR spectra were recorded to prove the successful functionalizations of PSDVB with PHEMA(-TMS) and PFMMA copolymer and block copolymer. Fig. 2a shows the spectra of PSDVB@CP-1 particles before and after deprotection of the TMS group, which were functionalized by statistical copolymerization of FMMA and HEMA-TMS. In addition, the ATR-IR spectrum of the PFMMA homopolymer is given for comparison. The spectra of PHEMA-TMS and PHEMA homopolymers can be found in Fig. S1. The characteristic IR signals of PSDVB particles [76] and the polymers were observed in both copolymer-functionalized particles verifying the modification of the particles. Thereby, the carbonyl group at 1725 cm^{-1} and the -C-O stretching band of the ester at 1141 cm^{-1} should be noted. The major difference was found in the -Si-O bond and the -Si-C bond observed at 841 cm^{-1} and 1250 cm^{-1}, respectively for the PSDVB@CP-TMS-1 particles. Moreover, the -C-O bond of primary alcohols of the deprotected PSDVB@CP-1 particles was observed at 1077 cm^{-1}. Fig. 2b compares the IR spectra of the PSDVB@BCP-1 samples before and after deprotection with the particles modified only with the first block PHEMA-TMS. The PSDVB@FB-1 particles revealed the bonds of the grafted polymer in lower intensity beside the PSDVB signals. As expected, the block copolymer-modified particles revealed identical signals as the copolymer-functionalized samples.

The surface structure of the different particles was investigated by scanning electron microscopy (SEM) as depicted in Fig. 3. Images of the other particle batches and additional magnifications can be found in Figs. S2–S5. For the SEM measurements, the particles were dispersed in tetrahydrofuran and drop-coated to a copper grid. The grid was placed on carbon tape and sputtered with a 6 nm platinum layer.

The PSDVB@FB-1 particles exhibited a highly porous surface morphology without a dense polymer coating on the particles' surface. This was due to a slight functionalization with PHEMA-TMS. In contrast, the block copolymer PSDVB@BCP-TMS-1 revealed a formation of a coating due to a higher degree of functionalization after adding of the second polymer block. A slight difference in the coating formation was observed after deprotecting of PHEMA-TMS functionalization, based on providing another kind of polymer [76]. These differences could be attributed to intermolecular interactions between the functional groups of the polymer. For example, the deprotected polymers can form hydrogen bonds between the hydroxyl groups of PHEMA. Therefore, the PSDVB@BCP-TMS particles exhibited a significantly smoother surface, while the coating of the deprotected PSDVB@BCP featured a more contoured surface. The capability of synthesizing block copolymers proves the living character of the SI-LAP process, which was also responsible for the homogeneous polymer coating. As a result, the high monodispersity of the microparticles could be maintained. As described previously [76], the thickness of the polymer coating correlated with the degree of functionalization. This could be observed using the PSDVB@BCP-TMS-2 particles with a higher degree of functionalization based on a higher amount of monomer used (Fig. S4a). Additionally, the thicker polymer coating results in slight amounts of polymer film between the contact areas of the single particles by entanglement of the polymer chains. PSDVB@BCP-TMS-3 particles with the lowest degree of functionalization revealed no formation of a dense coating but maintained the porous particle structure (Fig. S5). The comparison between the different particle batches showed different particle sizes, which correlate with the degree of functionalization and increase from the first to the second block (Table S3).

In addition, energy-dispersive X-ray spectroscopy was performed to investigate the iron distribution of the particle samples. For this, the particles were directly placed on a carbon tape and sputtered with a platinum layer. Fig. 4 shows the different functionalization states of the PSDVB@BCP-1 particles. The spectra of the other polymer batches can be found in Figs. S6 and S7. Element distribution of iron, based on ferrocene, and silicon, based on the TMS protecting group, was of interest. After functionalization with the first block PHEMA-TMS, silicon was detected well-localized on the particle spots (K_α at 1.74 keV, Fig. 4a and d). The concentration was significantly increased by the subsequent addition of the second block, which could be proven semi-quantitatively using EDX (Fig. 4b and e). In addition, iron was detected on the particles, which was demonstrated by the K_α signal at 6.40 keV (Fig. 4e and f). After deprotection, the concentration of iron was maintained, while the concentration of silicon decreased significantly. However, traces of silicon were monitored after the deprotection process due to incomplete conversion of the deprotection reaction, as is to be expected for polymer analog reactions in general.

It can be assumed that the polymer was successfully covalently

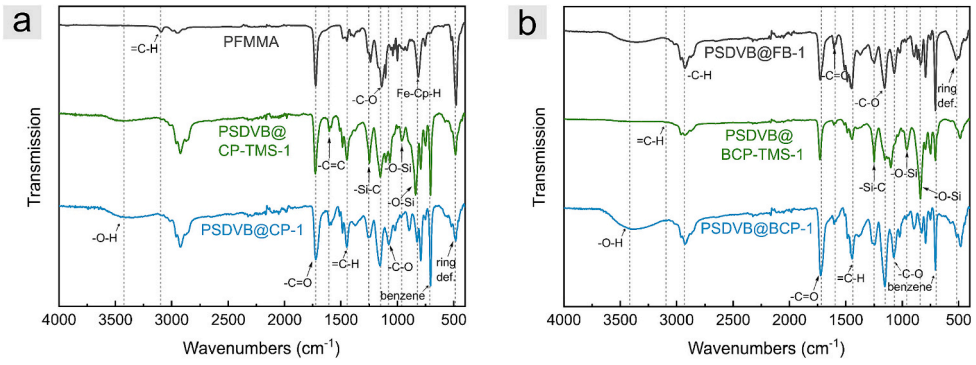

Fig. 2. Infrared spectroscopic data of a) PSDVB@CP-1 particles before (green) and after (blue) deprotection compared with PFMMA homopolymer (black) and b) PSDVB@BCP-1 particles before (green) and after (blue) deprotection compared to the particles modified only with the first block PHEMA-TMS (PSDVB@FB-1, black).

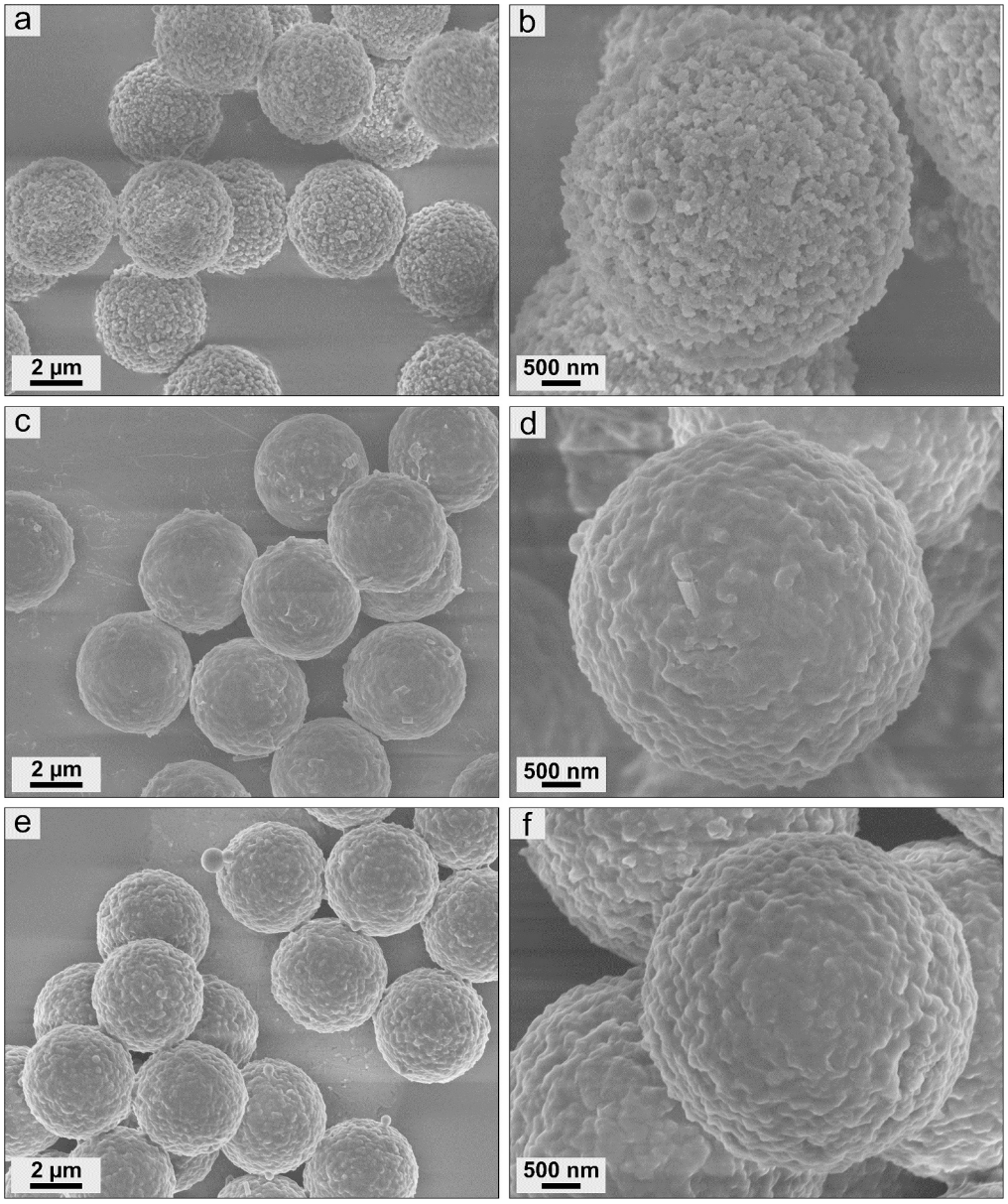

Fig. 3. Scanning electron microscopy images of a, b) PSDVB@FB-1, c, d) PSDVB@BCP-TMS-1, and e, f) PSDVB@BCP-1 particles in different magnifications.

attached within all particle batches. From the SEM investigations, it can be concluded that homogeneous microparticles without the formation of additional free polymer were obtained. The retention of the porous structure at low degrees of functionalization in combination with the localization of the polymer on the surface (Figs. 4 and S2–S7) confirmed this assumption. In addition, non-immobilized polymer residues could be removed by intensive multiple-washing processes. The particles presented here were washed more than 20 times and redispersed in different solvents to exclude the presence of non-immobilized polymer. All these combined investigations and results prove the presence of a covalent bond between the microparticles and the functional polymers.

3.2. *Electrochemical switchability*

The synthesized particles pave the way for a wide range of applications in the field of redox-responsive materials due to the covalent bond. Therefore, the stimuli-responsive behavior was investigated by studying the electrochemical addressability utilizing cyclic voltammetry. By considering both, the TMS-protected and the deprotected particles, the difference in electrochemical response and properties based on hydrophilization could be demonstrated. For these investigations, the particles were dispersed with multi-walled carbon nanotubes (MWCNT) to achieve a higher contact area between the particles and the electrically conductive electrode. By using the TMS-protected particles, sufficient interaction on a microscopic scale with MWCNTs could be obtained by mild ultrasonic treatment of the dispersion in ethanol (Figs. 5a and S8). In contrast, flocculation was observed in the mixture of OH-containing particles with MWCNTs based on a lack of miscibility at the microscale level (Figs. 5b and S9). Instead, the MWCNTs were deposited well separated from the particles due to the different polarities. Note that the particles can break under intensive ultrasonic treatment. For this reason, it was necessary to increase the dispersibility of the OH-containing particles with MWCNTs, e.g. by using phenol as an additive to achieve a better interaction (Figs. 5a–d and S10). The importance of miscibility at the microscale level was evident in cyclic voltammetric measurements without using phenol by preparation (Fig. S11). These cyclic voltammograms revealed a double signal due to the low interaction between the ferrocene units and the intrinsic conductive material which leads to

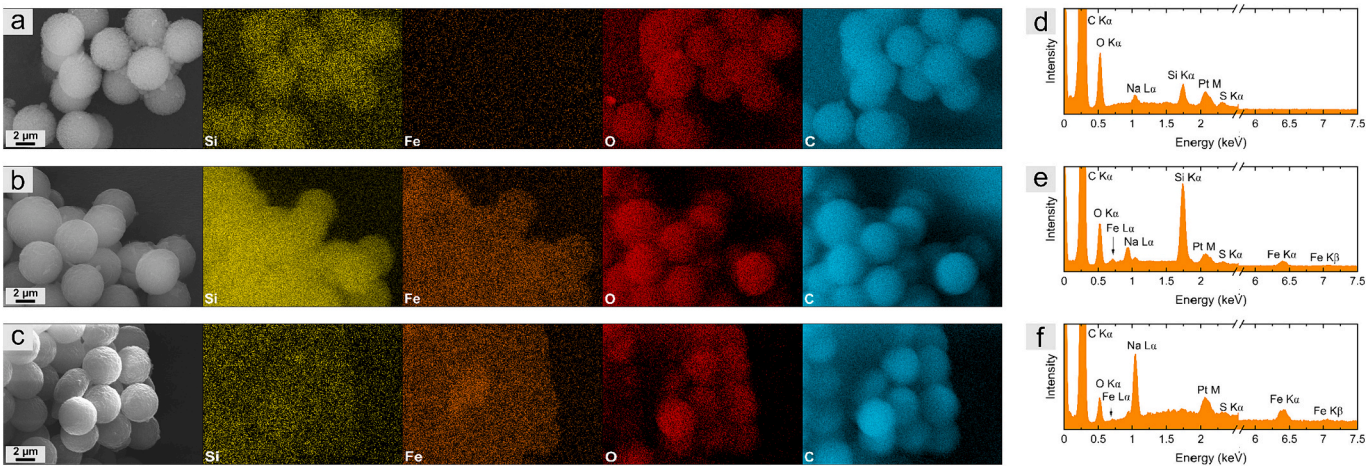

Fig. 4. Energy dispersive X-ray mapping of a) PSDVB@FB-1, b) PSDVB@BCP-TMS-1, and c) PSDVB@BCP-1 and representative energy dispersive X-ray spectroscopy point spectra of d) PSDVB@FB-1, e) PSDVB@BCP-TMS-1, and f) PSDVB@BCP-1, respectively.

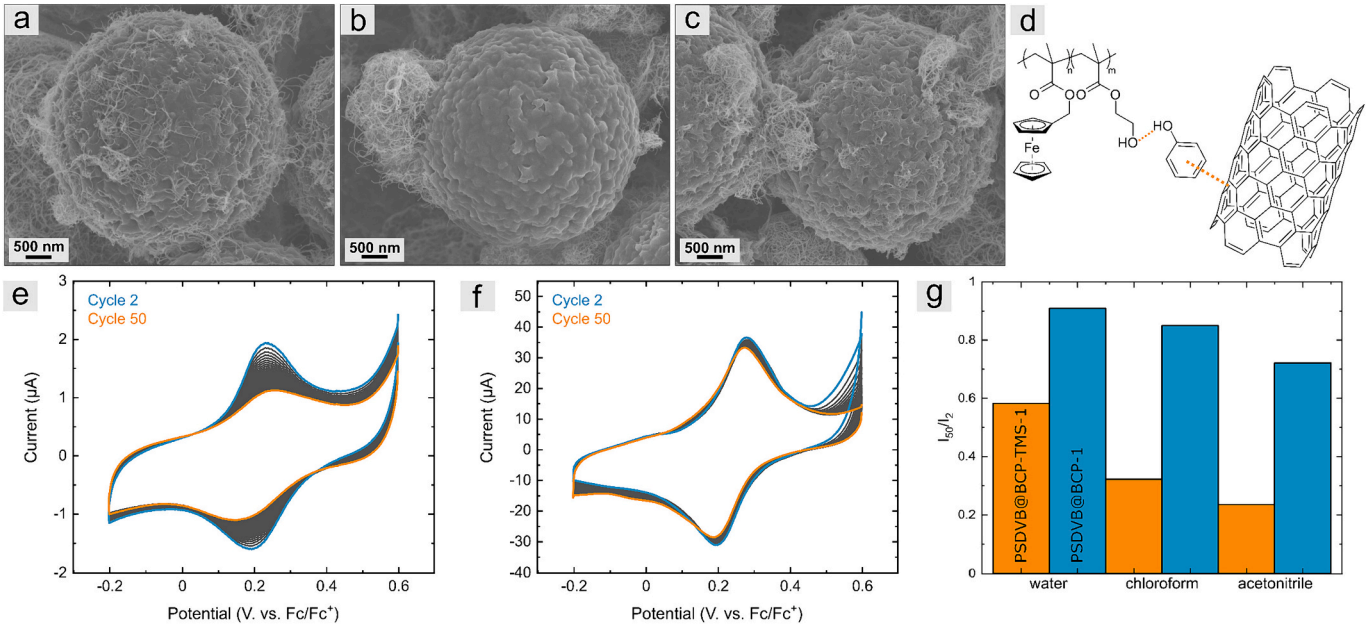

Fig. 5. Scanning electron microscopy images of a) PSDVB@BCP-TMS-1 mixed with MWCNTs, b) PSDVB@BCP-1 mixed with MWCNTs, and c) PSDVB@BCP-1 mixed with MWCNTs in the presence of phenol. d) Schematic structure of interaction of the particles with phenol and MWCNTs. e–g) Cyclic voltammetry investigation of e) PSDVB@BCP-TMS-1, and f) PSDVB@BCP-1 in water using $NaClO_4$ (0.1 M) as electrolyte with a scan rate of 20 mV s^{-1}. The second and the 50 cycles are marked as guides for the eyes only. g) Difference in measurement stability of the block copolymer-functionalized particles without (orange) and with hydroxy group (blue) in different media. The corresponding cyclic voltammograms and cyclic voltammograms of phenol only in the investigated potential range for comparison can be found in Fig. S11.

secondary effects. For the measurements, the MWCNT-particle dispersions were drop-coated onto a GC electrode and measured in different media. Fig. 5e and f demonstrate the cyclic voltammograms of PSDVB@BCP-TMS-1 and PSDVB@BCP-1 in water with $NaClO_4$ as an electrolyte. For better comparison, the TMS-protected particles were prepared with phenol by dispersion, too.

In both cases, the electrochemical addressability of the particles could be demonstrated. However, the significantly stronger decrease in signal intensity with an increasing number of measurements for the TMS-protected particles was noteworthy. In an aqueous solution, the TMS-protective particles maintained 58 % of the signal intensity after 50 cycles, while the hydroxylated material maintained 91 %. This behavior was also observed in other organic solvents like chloroform and acetonitrile using tetrabutylammonium hexafluorophosphate as an electrolyte (Fig. S11). Fig. 5g displays the ratio of the maximum currents of the second and the 50 cycles of both particle kinds in the various solvents. The higher decrease of the signal intensity of the hydrophobic PSDVB@BCP-TMS-1 compared to the hydroxy-group-containing derivates could be recognized in the different media. In general, various effects can play a role in the stability of the measurements. Recently, it has been demonstrated that incorporating hydrophilic comonomers into PVFc can enhance its electrochemical stability [81]. Furthermore, it is described in the literature [82] that the solubility effects of investigated materials can lead to detachment from the working electrode and thus to a decrease in signal intensity. The polymer coating of particles can in principle affect the interaction of the particles with the MWCNTs and the electrodes respectively, also induced by swelling effects. However, SEM measurements after performing the electrochemical experiments did not

reveal a significant alteration of the particles (Fig. S12), and strong π–π-interactions between ferrocene and MWCNTs are still assumed to result in stable mixtures [83]. It can be furthermore assumed, that the higher polarity of the deprotected polymer coating has a stronger effect because it increases the interaction of ferrocene moieties in the hydrophilic copolymer and the ionic electrolyte solution. It also reduces the *osmotic shock* situation within the polymer brush, leading to higher cyclic stability.

These studies demonstrate the importance of the polarity of redox-responsive materials and the targeted design of such polymer-coated surfaces. The findings are not limited to aqueous electrolytes but also apply to ionic electrolytes in organic solvents. It is expected that these findings will lead to improved redox-responsive materials, which play a crucial role for example in separation processes or sensing materials.

3.3. Ion adsorption and ion exchange

Ion adsorption and ion exchange experiments were carried out to demonstrate the application of the particles as adsorbent materials. For this, the materials were first investigated by static adsorption measurements. The particles PSDVB@BCP-2 with the highest ferrocene content and the PSDVB@CP-1, both with and without TMS protective groups were considered to investigate the direct influence of the hydroxy groups. In addition to the statistical co- and block copolymer-functionalized particles, the PFMMA homopolymer-functionalized particles (PSDVB@PFMMA) were analyzed for comparison studies. To oxidize the materials, iron chloride hexahydrate in acetonitrile was used as an oxidation solution. After multiple washing cycles to remove the excess chloride and drying under an argon atmosphere, the particles were dispersed in an aqueous sulfate solution for statical ion exchange and adsorption investigations. Sulfate was chosen as the ion for the exchange process due to its high content in the environment, particularly in the agricultural sector. On the other hand, as a divalent ion, it is entropically favored for interaction with ferrocenium compared to the counter ion chloride and it provides a suitable model for the investigation of potential advantages that can be gained through hydrophilization in analytical applications [21]. Sodium was chosen in all experiments as a counterion to the salts to avoid any additional effects of different cations. First, the stability of the chemically oxidized particles as a function of time was examined and is displayed in Fig. 6a.

The capacity of the ion adsorption processes was reduced over time in all cases. It can be assumed, that this could be probably due to a reduction process of ferrocenium to ferrocene in water or other side reactions, which can be observed in aqueous solutions without the presence of an oxidizing reagent (after washing process). Furthermore, the stability of the capacity was strongly decreased in the cases of TMS-protective co- and block copolymers (47–65 %) compared to a much higher stability of ~80 % during 2 h in aqueous environment by the PHEMA-containing polymers (Fig. 6b). The PFMMA homo polymer-functionalized particles revealed a stability of 66 % and thus exhibited reduced stability compared to the hydrophilized block copolymer particles, too. These studies demonstrated the positive effect of the OH groups and confirmed the results of the electrochemical investigation. An overview of the total capacities of the individual particle batches is given in Figs. 7a and S13. For better comparability, the values were normalized to the ferrocene content, which was determined using ICP-OES measurements (Table S2). Comparison of identical particle batches with and without TMS protecting group revealed thereby a higher absorption capacity of the hydroxylated particles. There are multiple reasons for this: (*i*) flocculation of the hydrophobic particles in acetonitrile and water occurred (Fig. S13a), which could lead to a reduction in the capacity of oxidized ferrocenium groups. In addition, the diffusion during the adsorption process in water may have been reduced by the flocculation. (*ii*) Through hydrophilic groups, a higher overall swellability of the particles in water could take place [84,85] which paves the way for higher addressability of the functionalized groups within the particle pores. (*iii*) The exchange of ions within a polymer brush can affect the brush swelling at a molecular level, causing changes in the osmotic pressure on the polymer chains within a polyelectrolyte brush. For example, it is well known that the osmotic pressure within a polymer brush can be modulated by using multivalent ions compared to single valent ions [63,86]. The effect on the osmotic pressure within the brush, which may lead to *entropic death* of the polymer chains [87–89], could be reduced using hydrophilized polyelectrolyte brushes and lead to increased stability. (*iv*) The OH groups could facilitate adsorption compared to the TMS groups by forming hydrogen bonds to the sulfate ions. Comparative studies with non-functionalized PSDVB particles revealed thereby no ion adsorption (Fig. S13b), which proves that the ion adsorption did not only occur through the particulate structure but through the ferrocenium groups. The separation efficiency of the particles was determined for the PSDVB@PFMMA particles to be 89.34 ± 0.03 % due to sorption measurements by different particle concentrations (excess).

For investigation of the ion adsorption regarding different anions, the experiments were carried out with stock solutions of fluoride and nitrate, respectively. In accordance with the sulfate solution, 10 mg·L^{-1} solutions were provided in both cases. First, we investigated the selectivity of three types of particles containing TMS-groups (PSDVB@BCP-TMS-2), hydroxy-groups (PSDVB@BCP-2), and PFMMA homopolymer (PSDVB@PFMMA). The PSDVB@PFMMA particles revealed the lowest adsorption capacity for nitrate (119 mg·g_{Fc}^{-1}), while fluoride and sulfate exhibited similar values with 189 and 200 mg·g_{Fc}^{-1} (Fig. 7b). In contrast, the PSDVB@BCP-TMS particles were found to have a higher capacity for nitrate (117 mg·g_{Fc}^{-1}) than for sulfate (66 mg·g_{Fc}^{-1}) or fluoride (89 mg·g_{Fc}^{-1}). It can be assumed, that the preference for nitrate was observed because of a stronger interaction with the particles on short timescales due to the polarizable character of the nitrate compared to the other ions. This behavior is well known in the literature for non-hydrophilized

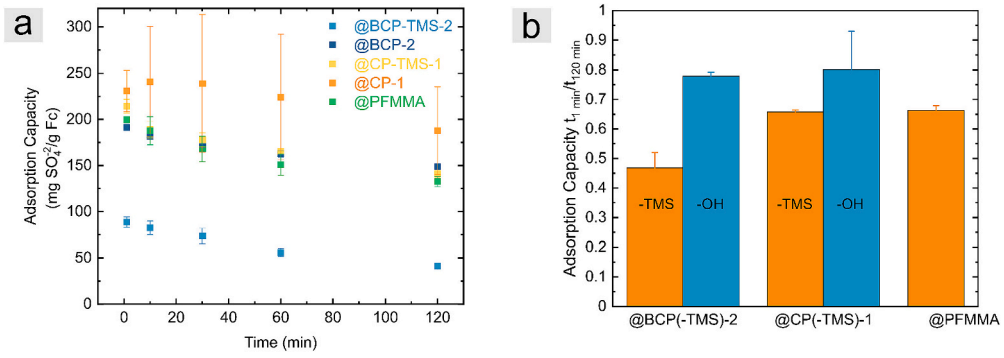

Fig. 6. a) Adsorption capacities of sulfate depending on time after oxidation with iron chloride hexahydrate in static measurements, and b) ratio of sulfate adsorption capacity after 1 min and after 120 min of the different functionalized particles.

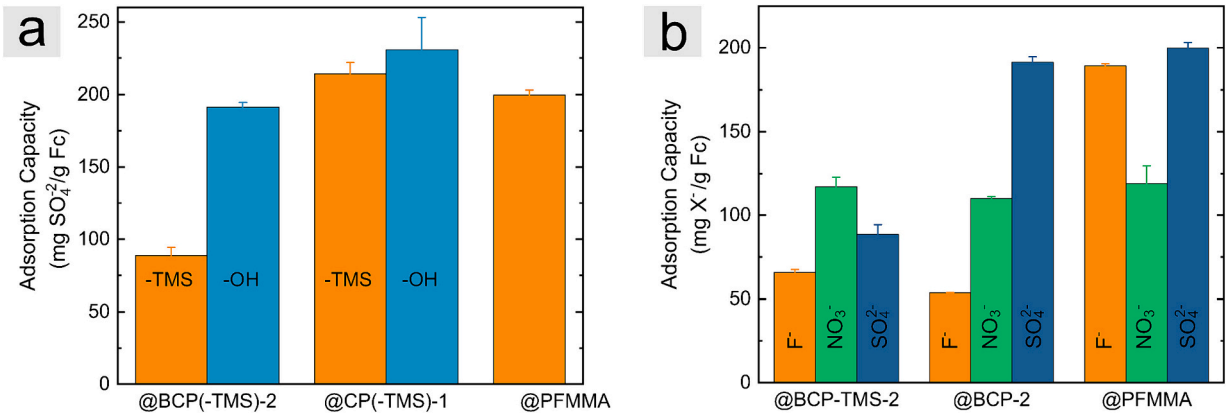

Fig. 7. Adsorption capacity measured in static experiments after oxidizing with iron chloride hexahydrate. a) Comparison of different functionalized PSDVB particles with TMS-protecting group versus deprotected hydroxy groups regarding the sulfate adsorption after 1 min and b) adsorption capacities of the different particles in three different ion solutions containing fluoride ions, nitrate ions, or sulfate ions. All capacities were normalized to the ferrocene content of the particles.

amine-functionalized particles [24,90] and represents a major reason for the necessity of hydrophilization of such particles for analytical applications. The hydrophilized BCP-functionalized particles exhibited significantly higher adsorption of sulfate (191 mg·g_{Fc}^{-1}) in comparison to fluoride (54 mg·g_{Fc}^{-1}) and nitrate (110 mg·g_{Fc}^{-1}). Electrochemical studies of ferrocene polymers in literature displayed mostly a higher adsorption capacity for hydrophobic homopolymers compared to hydrophilic copolymers [55,56]. The particles prepared in this study demonstrated this behavior for example for the ion fluoride, which was more adsorbed by the homopolymer-, but less by the copolymer-functionalized materials. The direct comparison of TMS-protective versus deprotected particles indicated, that not only the hydrophilization but rather the incorporation of comonomers could play a role in this, which affect directly the polymer brush structure. In the case of particles, various factors may influence the osmotic pressure within the polymer chain, which can have a significant impact. For example, the charge density can be reduced strongly due to the incorporation of comonomers, resulting in different brush behavior on the surfaces [88]. However, the direct influence of hydrophilicity can be recognized by the adsorption of sulfate which was significantly different for the TMS-protected and deprotected particles. As already indicated above, the formation of hydrogen bonds between sulfate and the hydroxy group of PHEMA could be a reason for the higher adsorption of sulfate. In addition, the hydrophilization can lead to a higher addressability of the ferrocene groups within the pores in aqueous environment. The influence of the porosity of the materials was evident through the high capacities (up to 200 mg·g_{Fc}^{-1}) for different particle batches compared to non-immobilized polymers, which proves the advantage of highly porous and accessible particles. Based on the data for other ions known from the literature [55,56], it can be assumed that the hydrophilization of the ferrocene polymers itself was not accountable for the higher capacities, but rather the combination between the particulate structure and the accessibility of the ferrocene groups within the pores.

Due to their high porosity, the polystyrene particles functionalized using SI-LAP were especially suitable for flow-through measurements (Fig. 8). For these studies, we investigated firstly the ion exchange by using the PSDVB@PFMMA homopolymer-functionalized material. The particles were embedded in a syringe cannula between two glass

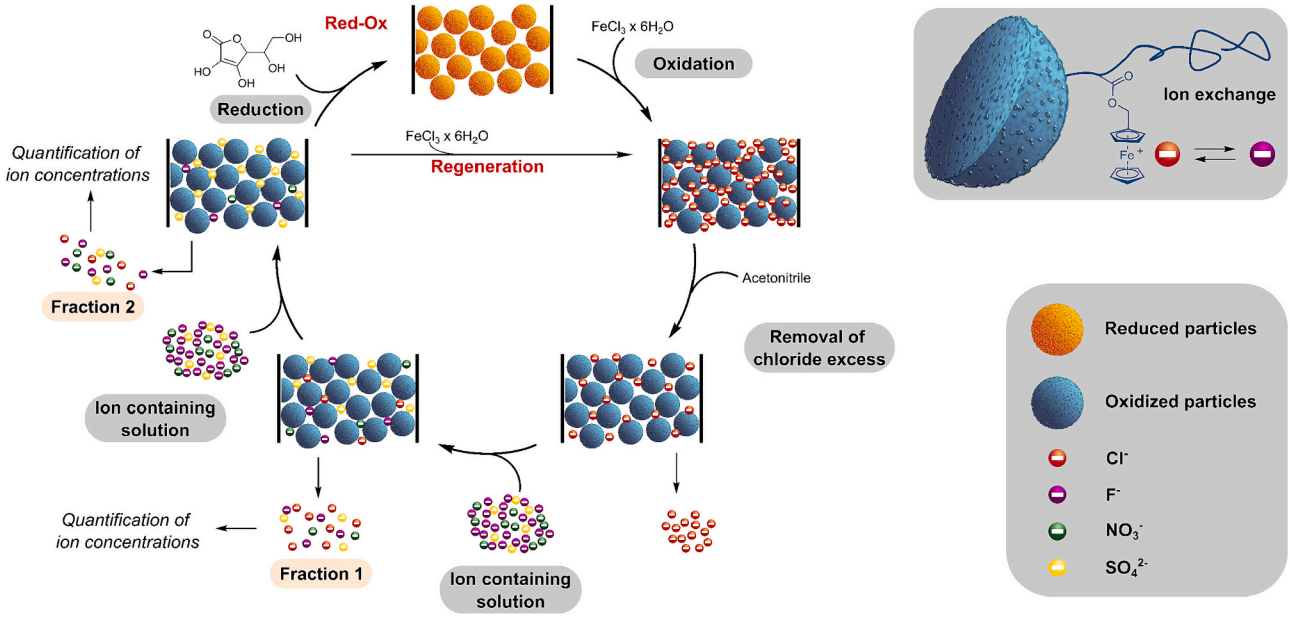

Fig. 8. Principles of ion adsorption and exchange flow experiments, highlighting the difference between "Regeneration" and "Red-Ox" experiments. In the "Regeneration" experiment, the exchange materials were rinsed with iron chloride after each cycle to restore their initial state, whereas in the "Red-Ox" experiment, the exchange materials were reduced and oxidized after each cycle.

microfiber filters and oxidized in flow with an excess of iron chloride hexahydrate resulting in a color change of the particles (Fig. S14).

A multi-ion solution containing fluorides (~5 mg·L^{-1}), nitrates (~5 mg·L^{-1}), and sulfate (~4 mg·L^{-1}) was pumped through the particle-containing cannula (~2–4 mg particles per experiment) with a flow rate of 3.5 mL·min^{-1} and analyzed in five fractions (Fig. 9a). In each fraction, 5 mL of solution was used, and ~97 % of the solution volume was retrieved. The first fraction contained a significant excess of chloride ions, which is attributed to the oxidation process and could not be completely removed by the washing cycles. In the following fractions, the chloride content decreased continuously indicating a successful ion exchange mechanism. In fraction one, all three ions provided were adsorbed (20 mg·g$_{Fc}^{-1}$ fluoride, 35 mg·g$_{Fc}^{-1}$ nitrate, and 33 mg·g$_{Fc}^{-1}$ sulfate). The second fraction revealed further adsorption of 33 mg·g$_{Fc}^{-1}$ sulfate and 19 mg·g$_{Fc}^{-1}$nitrate, while the fluoride content of the solution corresponds approximately to the initial concentration. The third fraction exhibited sulfate as an adsorbed ion, while the concentrations of fluoride and nitrate increased slightly (0.3 mg·g$_{Fc}^{-1}$ fluoride and 1.4 mg·g$_{Fc}^{-1}$ nitrate). This increase of ions in the solution can be observed in later fractions after the adsorption capacity of the materials was reached. Fig. 9b shows the capacity of the different fractions, which decreased as expected due to the maximum capacity of the ionic groups being reached. Additionally, an overview of the percentage adsorption amount can be found in Fig. S15. In fractions four and five the concentration of nitrate in the remaining solution was significantly increased (12 and 9 mg·g$_{Fc}^{-1}$), demonstrating the ion exchange process of nitrate with sulfate. The order of the ion exchange rate $F^- > NO_3^- > SO_4^{2-}$ corresponded to the order known in the literature for these anions in classical ion adsorption experiments with amine-functionalized particles [23,24]. Note, that comparative studies with non-functionalized PSDVB particles have found to adsorb none of the ions significantly. To investigate the influence of the flow-through principle versus static measurements on the total capacity, PSDVB@PFMMA particles were also tested regarding their capacity in the multi-ion solution using static experiments similar to those described above. This resulted in slightly higher capacities in the static measurement, which can, however, be attributed to the decrease in capacity over time (Fig. 6a). A high total capacity of 176 mg·g$_{Fc}^{-1}$ was achieved via a flow-through system (Fig. 9c). Even though the flow rate of 3.5 mL·min^{-1} was rather high for ion chromatography, the selectivity was still significant, and the capacities were also remarkable, making the developed material platform attractive to several industrial applications.

Cyclic stability measurements were carried out over five adsorption cycles. Two experimental routes were employed for this purpose (Fig. 8). The first method was the regeneration technique, in which the ferrocene units were rinsed with a more concentrated iron chloride solution at the end of a cycle. The counterions were replaced by chloride and the reduced ferrocene groups could be oxidized again. This corresponds to the classical method in ion chromatography for particles containing e.g. amine groups. The second method was the "Red-Ox" technique, in which the stimuli-responsive behavior of the ferrocenes was exploited. The bound ions were desorbed by reducing the ferrocenium groups to neutrally charged ferrocenes. Subsequent oxidation returned the ion exchangers to their initial state. For both methods, the multi-ion solution containing fluoride (~5 mg·L^{-1}), nitrate (~5 mg·L^{-1}), and sulfate (~4 mg·L^{-1}) was first pumped through the particle-containing cannula with a flow rate of 3.5 mL·min^{-1} and analyzed in two fractions of 5 mL. As a result of the single-ion investigations, the sulfate ion was chosen to be contained in a slightly lower concentration to examine the selectivity of hydroxy-groups containing polymer-functionalized particles for sulfate. The particles were afterward regenerated by using an iron chloride hexahydrate solution and the excess oxidation agent was removed by a washing cycle. In this process, renewed oxidation of any reduced particles was ensured. The experiments were conducted using the PSDVB@PFMMA homopolymer-functionalized particles (Fig. 10a and d), the block copolymer-functionalized particles PSDVB@BCP-TMS-2 (Fig. 10b and e), and PSDVB@BCP-2 (Fig. 10c and f). A comparison of the total capacities revealed that the capacity of PSDVB@PFMMA particles decreased to 65 % in the first two fractions. The protected BCP-TMS particles remained at an even lower capacity of 59 %, which confirmed the results of the time-dependent measurements above. The hydrophilic particles demonstrated a much higher stability by remaining a capacity of 82 %. However, it should be noted, that the first cycle generally exhibits the highest deviations and that subsequently a higher cycle stability can be achieved. Moreover, it was evident, that the presence of hydrophilic groups affected the ion exchange process. The amount of sorbed anions using PSDVB@PFMMA particles in the first fraction possessed ~60–82 % with a high degree of discontinuity. The PSDVB@BCP-TMS-2 particles revealed a higher regularity after the first cycle, but a similar low amount of sorbed anions in the first fraction (70–78 %). In contrast to this, the hydrophilic PSDVB@BCP-2 particles demonstrate a higher percentage ratio of 85–93 % indicating a faster ion exchange process. This finding was confirmed by analyzing the composition of anions in the first fraction (Fig. 10c, f). The hydrophilized particles adsorbed mostly sulfate ions (58–76 %), which suggests that the ion exchange process with the divalent ion occurred already. In addition, the measurements exhibited a relatively high uniformity of adsorption during the 5 cycles. In comparison, the same particles containing the TMS protective group revealed lower sulfate adsorption and higher nitrate capture. The PFMMA homopolymer-functionalized particles were found to have the lowest adsorption of sulfate in the first fraction down to 13 %, but therefore a higher adsorption of fluoride and nitrate. The second fractions of the PSDVB@PFMMA particles mainly contained sulfate, while nitrate and fluoride were desorbed (Fig. S16).

In addition to investigating the potential applications of ion adsorption materials and the benefits of hydrophilization, the study explored the possibility of utilizing redox-responsive characteristics. Because of the more distinguishable differences in fractions for short flow distances, the PSDVB@PFMMA particles were chosen for proof-of-

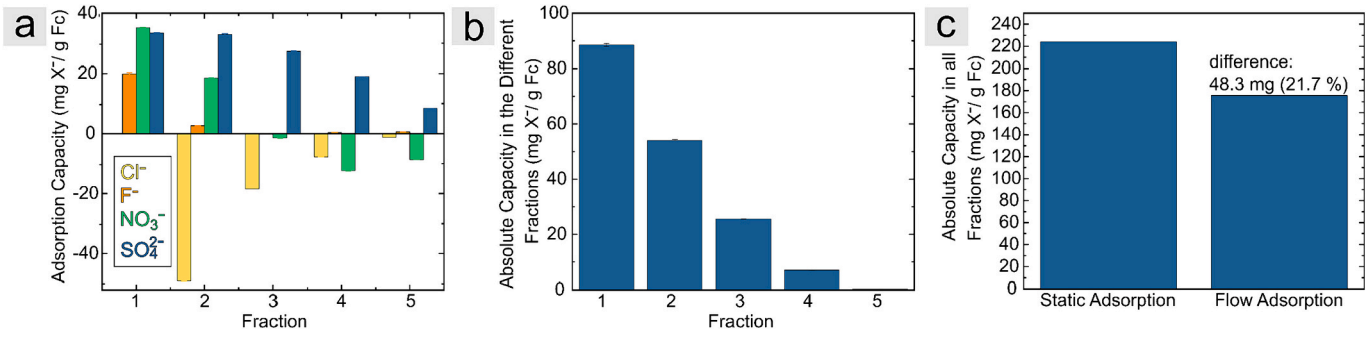

Fig. 9. a) Adsorption capacity of PSDVB@PFMMA in the multi-ion mixture observed in flow-through experiments by analyzing 5 fractions, b) the corresponding overall capacity, and c) the difference in capacity by static versus flow-through experiments.

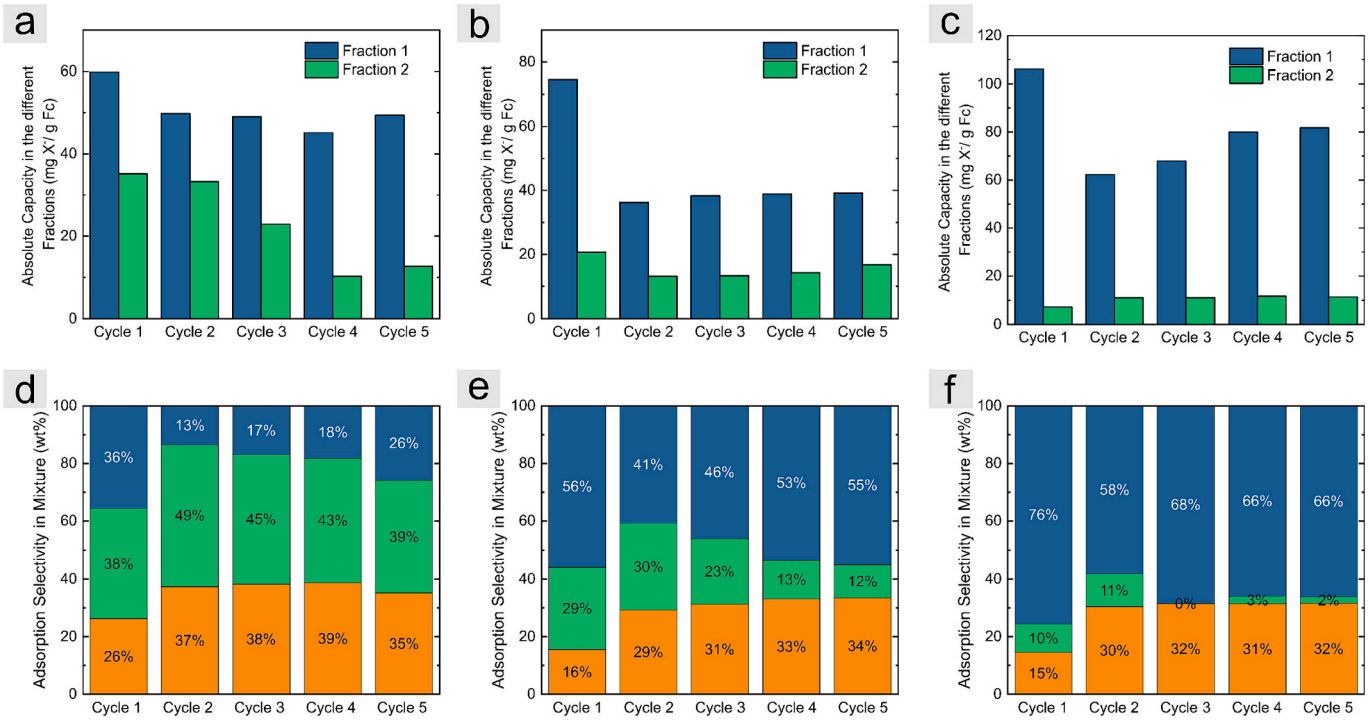

Fig. 10. Adsorption studies utilizing the regeneration flow-through principle with a, d) PSDVB@PFMMA, b, e) PSDVB@BCP-TMS-2, and c, f) PSDVB@BCP-2. a–c) Adsorption capacities of two fractions (fraction one in blue and fraction two in green) within five cycles normalized to the ferrocene content, and d-f) content of adsorbed ions in the first fractions. The second fraction can be found in Fig. S16. Fluoride content is displayed in orange, nitrate in green, and sulfate in blue. The stock solution contained 35.5 % fluoride (~5 mg·L^{-1}), 35.5 % nitrate (~5 mg·L^{-1}), and 30 % sulfate (~4 mg·L^{-1}).

concept studies (Fig. 11). This study utilized a Red-Ox process (Fig. 8), in which the particles were reduced due to flow-through with ascorbic acid in deionized water (0.1 M) after each adsorption cycle. This was followed by renewed oxidation using iron chloride hexahydrate. As the highest adsorption capacity was observed in fractions one and two, two ion exchange fractions were analyzed in each cycle before reducing the material. It was found that the material has a high capacity for adsorbing nitrate and fluoride comparably to the regeneration process (Fig. S17). However, there were major differences in the cyclic stability of the material, as seen in Fig. 11a. Specifically, there was a noticeable decrease in adsorption capacity during the five cycles. The lack of stability of this process can be attributed to several aspects: (*i*) ascorbic acid, which was used as a reducing agent, could have remained/accumulated in the pores of the particles in too tiny amounts and thus influenced the measurements and the total capacity. This aspect would not be observed by electrochemically controlled flow applications and will therefore not be investigated further. (*ii*) The structure of polyelectrolyte brushes on the surface is in general determined by the intermolecular electrostatic interactions of the chains and the osmotic pressure within the brush, which is attributed to counterion condensation. The intensity of the osmotic pressure of a polyelectrolyte brush can be affected by several factors. In particular, the number of charges within the chain represents a significant intrinsic factor for this [88,91]. Due to the reduction of ferrocenium, the amount of positively charged groups decreased strongly, whereby the counter ions were driven out of the polymer brush following the charge gradient. In addition, a collapse

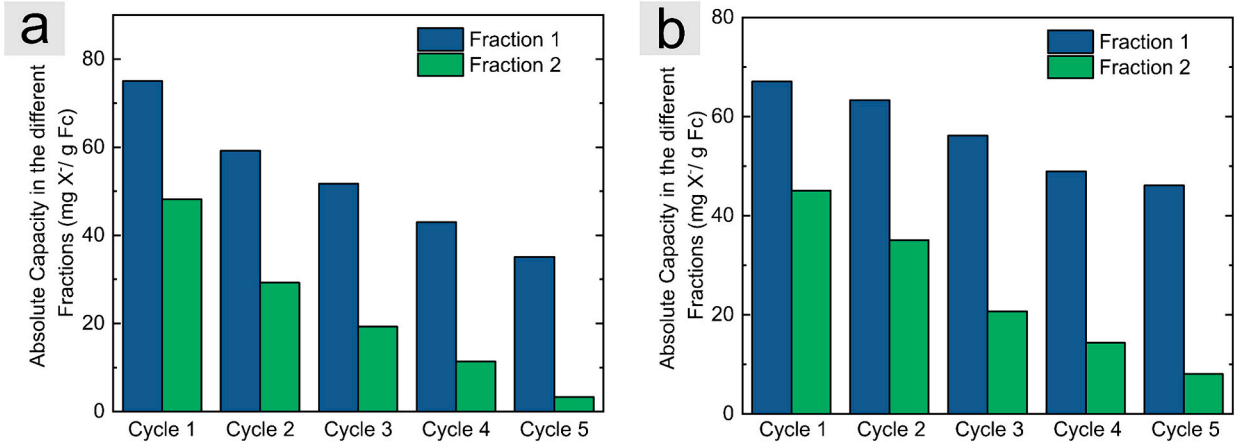

Fig. 11. Adsorption studies utilizing the Red-Ox flow-through principle on PSDVB@PFMMA particles. The adsorption capacities of two fractions (fraction one in blue and fraction two in green) within five cycles normalized to the ferrocene content is displayed, whereby the reductions were carried out in a) 0.1 M ascorbic acid solution in deionized water and b) 0.1 M ascorbic acid in 1.0 M NaCl solution.

of the chain conformation was induced, causing the polymer brush to collapse at a molecular level [88]. The quick change of the osmotic pressure within the brush could lead to an *osmotic shock* situation [87], which could result in the *entropic death* of the polymer chains or side chain units and therefore in a lack of stability during the following cycles. The intensity of the osmotic pressure can be modulated by extrinsic factors such as salt concentrations [87,92], so this hypothesis was assessed by using a salt-containing reduction solution of ascorbic acid in 1.0 M NaCl in water. Fig. 11b displays the capacity of the ion adsorption during the five cycles. Compared to the experiments without the presence of ionic strength during the reduction process, a significant improvement in stability of ~20 % was observed. This strongly implies that the effect of osmotic shock must be taken into account by using stimuli-responsive polyelectrolyte brushes.

Several factors such as osmotic shock and hydrophilization need to be considered for the application of stimuli-responsive polyelectrolyte brushes to be used in different fields of ion adsorption and ion analysis. The extent of osmotic shock can be significantly influenced by intrinsic factors such as charge density or hydrophilic groups as well as extrinsic factors such as salt concentration. Through the targeted design of stimuli-responsive surfaces, these factors can be modulated, and the applicability of the materials can be improved. Living anionic polymerization has proven to be a powerful method for the tailored functionalization of surfaces.

4. Conclusion

In conclusion, a synthetic route for surface functionalization of porous microparticles with functional copolymers and block copolymers was reported. As monomers, HEMA-TMS and redox-responsive FMMA were used. For specific surface design, surface-initiated anionic polymerization was applied which enabled block copolymerization featuring the living character for sequential anionic polymerization. The functionalized particles were characterized by ATR-IR verifying the different synthesis steps of the synthesis process. The surface morphology was investigated by SEM, while energy-dispersive X-ray spectroscopy confirmed the homogenous element distribution and therefore the uniform functionalization. In addition, a comparison of cyclic voltammetry measurements of protected and deprotected block copolymer-functionalized particles demonstrated the influence of polarity on cyclic stability. Furthermore, the materials could be applied as ion adsorption and ion exchange materials. In static measurements, the time-dependent stability was found to be higher for hydrophilic particles compared to their hydrophobic pendants, confirming the observations in CV. Additionally, a significantly higher capacity of sulfate adsorption was observed. In flow-through measurements, the application as ion exchange materials could be highlighted, whereby the ion exchange process could be demonstrated on homopolymer-functionalized particles. These materials exhibited a lower stability compared to hydrophilized materials, demonstrating the importance of incorporating hydrophilic groups, particularly for analytical applications. Furthermore, the investigation of the redox-responsive Red-Ox flow-through experiment revealed the significance of the modulation of the osmotic situation within the polyelectrolyte brush during the switching process. For these reasons, we expect that the findings described here have a high impact on the application of stimuli-responsive polyelectrolyte brushes as ion adsorption and ion exchange materials. In addition, the materials synthesized and presented have demonstrated the potential as ion exchange resins, facilitating their application in various fields of ion adsorption or analysis, e.g. in ion chromatography. The excellent cyclic stability, especially of the hydrophilized materials, enables electrochemical control of the application.

CRediT authorship contribution statement

Deborah Schmitt: Writing – review & editing, Writing – original draft, Visualization, Validation, Methodology, Investigation, Formal analysis, Data curation, Conceptualization. **Markus Gallei:** Writing – review & editing, Writing – original draft, Visualization, Validation, Supervision, Software, Resources, Project administration, Funding acquisition, Data curation, Conceptualization.

Declaration of competing interest

The authors declare that they have no known competing financial interests or personal relationships that could have appeared to influence the work reported in this paper.

Data availability

Data will be made available on request.

Acknowledgments

The authors thank Prof. Volker Presser from the Leibniz Institute for New Materials for the possibility of using SEM and EDS measuring devices. We thank Metrohm AG (Switzerland) for donating PSDVB particles.

Appendix A. Supplementary data

Supplementary data to this article can be found online at https://doi.org/10.1016/j.desal.2024.117674.

References

[1] H. Leinonen, J. Lehto, A. Mäkelä, Purification of nickel and zinc from waste waters of metal-plating plants by ion exchange, React. Polym. 23 (1994) 221–228.
[2] T. Mitchenko, P. Stender, N. Makarova, Optimation of sorption purification of industrial effluents, waste waters and technological solutions from polyvalent metal ions, Solvent Extr. Ion Exch. 16 (1998) 75–149.
[3] C.A. Lucy, Recent advances in ion chromatography: a perspective, J. Chromatogr. A 739 (1996) 3–13.
[4] J. Ramkumar, T. Mukherjee, Effect of aging on the water sorption and ion exchange studies on Nafion and Dowex resins: transition metal ions-proton exchange systems, Sep. Purif. Technol. 54 (2007) 61–70.
[5] M. Homayoonfal, A. Akbari, M.R. Mehrnia, Preparation of polysulfone nanofiltration membranes by UV-assisted grafting polymerization for water softening, Desalination 263 (2010) 217–225.
[6] S. Fox, Y. Oren, Z. Ronen, J. Gilron, Ion exchange membrane bioreactor for treating groundwater contaminated with high perchlorate concentrations, J. Hazard. Mater. 264 (2014) 552–559.
[7] M. Gomelya, T. Shabliy, I. Makarenko, A. Vakulenko, Efficiency of reverse osmosis and ion exchange in water purification from nitrates, J. Ecol. Eng. 23 (2022) 172–180.
[8] A. Peppas, K. Komnitsas, I. Halikia, Use of organic covers for acid mine drainage control, Miner. Eng. 13 (2000) 563–574.
[9] K.D. Wakeman, L. Erving, M.L. Riekkola-Vanhanen, J.A. Puhakka, Silage supports sulfate reduction in the treatment of metals- and sulfate-containing waste waters, Water Res. 44 (2010) 4932–4939.
[10] N. Mubarak, I. Hussain, M. Faisal, T. Hussain, M.Y. Shad, N.M. Abdel-Salam, J. Shabbir, Spatial distribution of sulfate concentration in groundwater of South-Punjab, Pakistan, water quality, Expo. Health 7 (2015) 503–513.
[11] S. Permeh, K. Lau, M. Duncan, R. Simmons, Identification of steel corrosion in alkaline sulfate solution by electrochemical noise, Mater. Corros. 72 (2021) 1456–1467.
[12] D. Zak, M. Hupfer, A. Cabezas, G. Jurasinski, J. Audet, A. Kleeberg, R. McInnes, S. M. Kristiansen, R.J. Petersen, H. Liu, T. Goldhammer, Sulphate in freshwater ecosystems: a review of sources, biogeochemical cycles, ecotoxicological effects and bioremediation, Earth Sci. Rev. 212 (2021).
[13] D.R. Van Stempvoort, J. Spoelstra, G. Bickerton, G. Koehler, B. Mayer, M. Nightingale, J. Miller, Sulfate in streams and groundwater in a cold region (Yukon Territory, Canada): evidence of weathering processes in a changing climate, Chem. Geol. 631 (2023).
[14] S.D. Alexandratos, D.W. Crick, Polymer-supported reagents: application to separation science, Ind. Eng. Chem. Res. 35 (1996) 635–644.
[15] K. Biswas, S. Ghosh, B. Basu, Ion-exchange resins and polypeptide supported catalysts: a critical review, Curr. Green Chem. 7 (2020) 40–52.
[16] J.C. Kraak, K.M. Jonker, J.K. Huber, Solvent-generated ion-exchange systems with anionic surfactants for rapid separations of amino acids, J. Chromatogr. 142 (1977) 671–688.
[17] J. Stahlberg, Retention models for ions in chromatography, J. Chromatogr. A 855 (1999) 3–55.

[18] K. Nagase, J. Kobayashi, A. Kikuchi, Y. Akiyama, M. Annaka, H. Kanazawa, T. Okano, Influence of graft interface polarity on hydration/dehydration of grafted thermoresponsive polymer brushes and steroid separation using all-aqueous chromatography, Langmuir 24 (2008) 10981–10987.
[19] R.K. Khamizov, V.A. Ivanov, A.A. Madani, Dual-temperature ion exchange: a review, React. Funct. Polym. 70 (2010) 521–530.
[20] T.N. Kasiyanova, A.D. Smolenkov, A.V. Pirogov, O.A. Shpigun, Synthesis of polymeric anion exchangers bearing dimethylhydrazine and alkylammonium functional groups and comparison of their chromatographic properties, J. Anal. Chem. 63 (2008) 41–45.
[21] M.C. Bruzzoniti, E. Mentasti, C.A. Pohl, J.M. Riviello, C. Sarzanini, Effect of ion-exchange site and eluent modifiers on the anion-exchange of carboxylic acids, J. Chromatogr. A 925 (2001) 99–108.
[22] S. Schöttner, H.-J. Schaffrath, M. Gallei, Poly(2-hydroxyethyl methacrylate)-based amphiphilic block copolymers for high water flux membranes and ceramic templates, Macromolecules 49 (2016) 7286–7295.
[23] A.V. Zatirakha, A.D. Smolenkov, A.V. Pirogov, P.N. Nesterenko, O.A. Shpigun, Preparation and characterisation of anion exchangers with dihydroxy-containing alkyl substitutes in the quaternary ammonium functional groups, J. Chromatogr. A 1323 (2014) 104–114.
[24] Z. Yang, Z. Li, F. Zhang, B. Yang, S. Zhang, A novel hydrophilic polymer-based anion exchanger grafted by quaternized polyethyleneimine for ion chromatography, Talanta 197 (2019) 199–203.
[25] T. Yamakawa, S. Ishida, M. Higa, Transport properties of ions through temperature-responsive charged membranes prepared using poly(vinyl alcohol)/poly(N-isopropylacrylamide)/poly(vinyl alcohol-co-2-acrylamido-2-methylpropane sulfonic acid), J. Membr. Sci. 250 (2005) 61–68.
[26] S. Chahardahmasoumi, M.N. Sarvi, S.A.H. Jalali, Modified montmorillonite nanosheets as a nanocarrier with smart pH-responsive control on the antimicrobial activity of tetracycline upon release, Appl. Clay Sci. 178 (2019).
[27] M. Mauro, S. Bellemin-Laponnaz, C. Cebrián, Metal-containing polymers as light-emitting and light-responsive materials and beyond, Chem. A Eur. J. 23 (2017) 17626–17636.
[28] Y. Chen, W. Wu, J. Yu, Y. Wang, J. Zhu, Z. Hu, Mechanical strong stretchable conductive multi-stimuli-responsive nanocomposite double network hydrogel as biosensor and actuator, J. Biomater. Sci. Polym. Ed. 31 (2020) 1770–1792.
[29] G.R. Whittell, M.D. Hager, U.S. Schubert, I. Manners, Functional soft materials from metallopolymers and metallosupramolecular polymers, Nat. Mater. 10 (2011) 176–188.
[30] J. Zhou, G.R. Whittell, I. Manners, Metalloblock copolymers: new functional nanomaterials, Macromolecules 47 (2014) 3529–3543.
[31] N. Casado, G. Hernández, H. Sardon, D. Mecerreyes, Current trends in redox polymers for energy and medicine, Prog. Polym. Sci. 52 (2016) 107–135.
[32] H. Kanazawa, T. Sunamoto, Y. Matsushima, A. Kikuchi, T. Okano, Temperature-responsive chromatographic separation of amino acid phenylthiohydantoins using aqueous media as the mobile phase, Anal. Chemistry 72 (2000) 5961–5966.
[33] K. Nagase, N. Kojima, M. Goto, T. Akaike, H. Kanazawa, Thermoresponsive block copolymer brush for temperature-modulated hepatocyte separation, J. Mater. Chem. B 10 (2022) 8629–8641.
[34] K. Nagase, J. Kobayashi, A. Kikuchi, Y. Akiyama, H. Kanazawa, M. Annaka, T. Okano, Preparation of thermoresponsive anionic copolymer brush surfaces for separating basic biomolecules, Biomacromolecules 11 (2010) 215–223.
[35] E. Ayano, K. Nambu, C. Sakamoto, H. Kanazawa, A. Kikuchi, T. Okano, Aqueous chromatography system using pH- and temperature-responsive stationary phase with ion-exchange groups, J. Chromatogr. A 1119 (2006) 58–65.
[36] M. Gallei, C. Rüttiger, Recent trends in metallopolymer design: redox-controlled surfaces, porous membranes, and switchable optical materials using ferrocene-containing polymers, Chem. A Eur. J. 24 (2018) 10006–10021.
[37] D. Astruc, Why is ferrocene so exceptional? Eur. J. Inorg. Chem. 2017 (2017) 6–29.
[38] G.R. Whittell, I. Manners, Metallopolymers: new multifunctional materials, Adv. Mater. 19 (2007) 3439–3468.
[39] L. Gan, J. Song, S. Guo, D. Jańczewski, C.A. Nijhuis, Side chain effects in the packing structure and stiffness of redox-responsive ferrocene-containing polymer brushes, European, Polym. J. 83 (2016) 517–528.
[40] M. Mazurowski, M. Gallei, J.Y. Li, H. Didzoleit, B. Stühn, M. Rehahn, Redox-responsive polymer brushes grafted from polystyrene nanoparticles by means of surface initiated atom transfer radical polymerization, Macromolecules 45 (2012) 8970–8981.
[41] J. Elbert, J. Mersini, N. Vilbrandt, C. Lederle, M. Kraska, M. Gallei, B. Stühn, H. Plenio, M. Rehahn, Reversible activity modulation of surface-attached Grubbs second generation type catalysts using redox-responsive polymers, Macromolecules 46 (2013) 4255–4267.
[42] X. Mao, W. Tian, J. Wu, G.C. Rutledge, T.A. Hatton, Electrochemically responsive heterogeneous catalysis for controlling reaction kinetics, J. Am. Chem. Soc. 137 (2015) 1348–1355.
[43] X. Su, H.J. Kulik, T.F. Jamison, T.A. Hatton, Anion-selective redox electrodes: electrochemically mediated separation with heterogeneous organometallic interfaces, Adv. Funct. Mater. 26 (2016) 3394–3404.
[44] X. Su, A. Kushima, C. Halliday, J. Zhou, J. Li, T.A. Hatton, Electrochemically-mediated selective capture of heavy metal chromium and arsenic oxyanions from water, Nat. Commun. 9 (2018).
[45] X. Su, K.-J. Tan, J. Elbert, C. Rüttiger, M. Gallei, T.F. Jamison, T.A. Hatton, Asymmetric faradaic systems for selective electrochemical separations, Energ. Environ. Sci. 10 (2017) 1272–1283.
[46] X. Sui, X. Feng, J. Song, M.A. Hempenius, G.J. Vancso, Electrochemical sensing by surface-immobilized poly(ferrocenylsilane) grafts, J. Mater. Chem. 22 (2012) 11261.
[47] T. Winter, X. Su, T.A. Hatton, M. Gallei, Ferrocene-containing inverse opals by melt-shear organization of core/shell particles, Macromol. Rap. Comm. 39 (2018) 1800428.
[48] D. Scheid, C. Lederle, S. Vowinkel, C.G. Schäfer, B. Stühn, M. Gallei, Redox- and mechano-chromic response of metallopolymer-based elastomeric colloidal crystal films, J. Mater. Chem. C 2 (2014).
[49] D.P. Puzzo, A.C. Arsenault, I. Manners, G.A. Ozin, Electroactive inverse opal: a single material for all colors, Angew. Chem. Int. Ed. 48 (2009) 943–947.
[50] X. Su, T.A. Hatton, Electrosorption at functional interfaces: from molecular-level interactions to electrochemical cell design, Phys. Chem. Chem. Phys. 19 (2017) 23570–23584.
[51] N. Kim, W. Oh, K.N. Knust, F. Zazyki Galetto, X. Su, Molecularly selective polymer interfaces for electrochemical separations, Langmuir 39 (2023) 16685–16700.
[52] J. Jeon, J. Elbert, C.H. Chung, J. Chae, X. Su, Chiral metallopolymers for redox-mediated enantioselective interactions, Adv. Funct. Mater. 33 (2023).
[53] P. Baldaguez Medina, V. Ardila Contreras, F. Hartmann, D. Schmitt, A. Klimek, J. Elbert, M. Gallei, X. Su, Investigating the electrochemically driven capture and release of long-chain PFAS by redox metallopolymer sorbents, ACS Appl. Mater. Inter. 15 (2023) 22112–22122.
[54] D. Schmitt, A. Schiesser, M. Gallei, Balance of hydrophilicity and hydrophobicity of stimuli-responsive metallopolymer-decorated organic particles, ACS Appl. Polym. Mater. 6 (2024) 2993–3002.
[55] K.J. Tan, S. Morikawa, A. Hemmatifar, N. Ozbek, Y. Liu, T.A. Hatton, Hydrophobicity tuned polymeric redox materials with solution-specific electroactive properties for selective electrochemical metal ion recovery in aqueous environments, ACS Appl. Mater. Inter. 15 (2023) 43859–43870.
[56] K.J. Tan, S. Morikawa, N. Ozbek, M. Lenz, C.R. Arlt, A. Tschope, M. Franzreb, T. A. Hatton, Redox polyelectrolytes with pH-sensitive electroactive functionality in aqueous media, Langmuir 39 (2023) 2943–2956.
[57] K.-J. Tan, S. Morikawa, K.R. Phillips, N. Ozbek, T.A. Hatton, Redox-active magnetic composites for anionic contaminant removal from water, ACS Appl. Mater. Inter. 14 (2022) 8974–8983.
[58] J.O. Zoppe, N.C. Ataman, P. Mocny, J. Wang, J. Moraes, H.-A. Klok, Surface-initiated controlled radical polymerization: state-of-the-art, opportunities, and challenges in surface and interface engineering with polymer brushes, Chem. Rev. 117 (2017) 1105–1318.
[59] X.-P. Wei, R.-Q. Zhang, L.-B. Wang, Y.-L. Luo, F. Xu, Y.-S. Chen, Novel multi-walled carbon nanotubes decorated with gold nanoparticles with poly(2-methacryloyloxyethyl ferrocenecarboxylate) grafted on to form organic–inorganic nanohybrids: preparation, characterization, and electrochemical sensing applications, J. Mater. Chem. C 7 (2019) 119–132.
[60] Q. Hu, D. Han, S. Gan, Y. Bao, L. Niu, Surface-initiated-reversible-addition–fragmentation-chain-transfer polymerization for electrochemical DNA biosensing, Anal. Chem. 90 (2018) 12207–12213.
[61] J. Elbert, M. Gallei, C. Rüttiger, A. Brunsen, H. Didzoleit, B. Stühn, M. Rehahn, Ferrocene polymers for switchable surface wettability, Organometallics 32 (2013) 5873–5878.
[62] R. Barbey, L. Lavanant, D. Paripovic, N. Schüwer, C. Sugnaux, S. Tugulu, H.-A. Klok, Polymer brushes via surface-initiated controlled radical polymerization: synthesis, characterization, properties, and applications, Chem. Rev. 109 (2009) 5437–5527.
[63] W.-L. Chen, R. Cordero, H. Tran, C.K. Ober, 50th Anniversary Perspective: polymer brushes: novel surfaces for future materials, Macromolecules 50 (2017) 4089–4113.
[64] E. Unsal, B. Elmas, B. Çağlayan, M. Tuncel, S. Patir, A. Tuncel, Preparation of an ion-exchange chromatographic support by a “grafting from” strategy based on atom transfer radical polymerization, Anal. Chem. 78 (2006) 5868–5875.
[65] M. Lillethorup, K. Torbensen, M. Ceccato, S.U. Pedersen, K. Daasbjerg, Electron transport through a diazonium-based initiator layer to covalently attached polymer brushes of ferrocenylmethyl methacrylate, Langmuir 29 (2013) 13595–13604.
[66] R. Chen, J. Feng, J. Jeon, T. Sheehan, C. Rüttiger, M. Gallei, D. Shukla, X. Su, Structure and potential-dependent selectivity in redox-metallopolymers: electrochemically mediated multicomponent metal separations, Adv. Funct. Mater. 31 (2021) 2009307.
[67] X. Su, J. Hübner, M.J. Kauke, L. Dalbosco, J. Thomas, C.C. Gonzalez, E. Zhu, M. Franzreb, T.F. Jamison, T.A. Hatton, Redox interfaces for electrochemically controlled protein–surface interactions: bioseparations and heterogeneous enzyme catalysis, Chem. Mater. 29 (2017) 5702–5712.
[68] X. Fan, Q. Zhou, C. Xia, W. Cristofoli, J. Mays, R. Advincula, Living anionic surface-initiated polymerization (LASIP) of styrene from clay nanoparticles using surface bound 1,1-diphenylethylene (DPE) initiators, Langmuir 18 (2002) 4511–4518.
[69] Q. Zhou, X. Fan, C. Xia, J. Mays, R. Advincula, Living anionic surface initiated polymerization (SIP) of styrene from clay surfaces, Chem. Mater. 13 (2001) 2465–2467.
[70] Q. Zhou, S. Wang, X. Fan, R. Advincula, J. Mays, Living anionic surface-initiated polymerization (LASIP) of a polymer on silica nanoparticles, Langmuir 18 (2002) 3324–3331.
[71] R. Advincula, Q. Zhou, M. Park, S. Wang, J. Mays, G. Sakellariou, S. Pispas, N. Hadjichristidis, Polymer brushes by living anionic surface initiated polymerization on flat silicon (SiOx) and gold surfaces: homopolymers and block copolymers, Langmuir 18 (2002) 8672–8684.
[72] G. Sakellariou, M. Park, R. Advincula, J.W. Mays, N. Hadjichristidis, Homopolymer and block copolymer brushes on gold by living anionic surface-initiated

polymerization in a polar solvent, J. Polym. Sci. Part A: Polym. Chem. 44 (2006) 769–782.
[73] N. Rubio, H. Au, H.S. Leese, S. Hu, A.J. Clancy, M.S.P. Shaffer, *Grafting from* versus *grafting to* approaches for the functionalization of graphene nanoplatelets with poly (methyl methacrylate), Macromolecules 50 (2017) 7070–7079.
[74] M. Sato, T. Kato, T. Ohishi, R. Ishige, N. Ohta, K.L. White, T. Hirai, A. Takahara, Precise synthesis of poly(methyl methacrylate) brush with well-controlled stereoregularity using a surface-initiated living anionic polymerization method, Macromolecules 49 (2016) 2071–2076.
[75] J. Elbert, H. Didzoleit, C. Fasel, E. Ionescu, R. Riedel, B. Stühn, M. Gallei, Surface-initiated anionic polymerization of [1]Silaferrocenophanes for the preparation of colloidal preceramic materials, Macromol. Rapid Commun. 36 (2015) 597–603.
[76] D. Schmitt, S.M. Abdel-Hafez, M. Tummeley, V. Schünemann, M. Schneider, V. Presser, M. Gallei, Surface-initiated living anionic polymerization of functional methacrylates from the surface of organic particles, Macromolecules 56 (2023) 7086–7101.
[77] G.R. Fulmer, A.J.M. Miller, N.H. Sherden, H.E. Gottlieb, A. Nudelman, B.M. Stoltz, J.E. Bercaw, K.I. Goldberg, NMR chemical shifts of trace impurities: common laboratory solvents, organics, and gases in deuterated solvents relevant to the organometallic chemist, Organometallics 29 (2010) 2176–2179.
[78] R.B. Bates, L.M. Kroposki, D.E. Potter, Cycloreversions of anions from tetrahydrofurans. Convenient synthesis of lithium enolates of aldehydes, J. Org. Chem. 37 (1972) 560–562.
[79] P. Stanetty, M.D. Mihovilovic, Half-lives of organolithium reagents in common ethereal solvents, J. Org. Chem. 62 (1997) 1514–1515.
[80] C.J. Kim, K. Sondergeld, M. Mazurowski, M. Gallei, M. Rehahn, T. Spehr, H. Frielinghaus, B. Stühn, Synthesis and characterization of polystyrene chains on the surface of silica nanoparticles: comparison of SANS, SAXS, and DLS results, Coll. Polym. Sci. 291 (2013) 2087–2099.
[81] K.J. Tan, S. Morikawa, T.A. Hatton, Electroactive behavior of adjustable vinylferrocene copolymers in electrolyte media, J. Phys. Chem. B 128 (2024) 1748–1759.
[82] S. Moreno, H. Hübner, C. Effenberg, S. Boye, A. Ramuglia, D. Schmitt, B. Voit, I. M. Weidinger, M. Gallei, D. Appelhans, Redox- and pH-responsive polymersomes with ferrocene moieties exhibiting peroxidase-like, chemoenzymatic activity and H_2O_2-responsive release behavior, Biomacromolecules 23 (2022) 4655–4667.
[83] X. Mao, G.C. Rutledge, T.A. Hatton, Polyvinylferrocene for noncovalent dispersion and redox-controlled precipitation of carbon nanotubes in nonaqueous media, Langmuir 29 (2013) 9626–9634.
[84] G. Zheng, H.D.H. Stöver, Grafting of poly(alkyl (meth)acrylates) from swellable poly(DVB80-co-HEMA) microspheres by atom transfer radical polymerization, Macromolecules 35 (2002) 7612–7619.
[85] S. Schöttner, R. Hossain, C. Rüttiger, M. Gallei, Ferrocene-modified block copolymers for the preparation of smart porous membranes, Polymers 9 (2017) 491.
[86] Q.-H. Hao, G. Xia, H.-G. Tan, E.-Q. Chen, S. Yang, Surface morphologies of spherical polyelectrolyte brushes induced by trivalent salt ions, Phys. Chem. Chem. Phys. 20 (2018) 26542–26551.
[87] M. Menzel, W.L. Chen, K. Simancas, H. Xu, O. Prucker, C.K. Ober, J. Rühe, Entropic death of nonpatterned and nanopatterned polyelectrolyte brushes, J. Polym. Sci. A Polym. Chem. 57 (2019) 1283–1295.
[88] C.J. Galvin, E.D. Bain, A. Henke, J. Genzer, Instability of surface-grafted weak polyacid brushes on flat substrates, Macromolecules 48 (2015) 5677–5687.
[89] W.-L. Chen, M. Menzel, O. Prucker, E. Wang, C.K. Ober, J. Rühe, Morphology of nanostructured polymer brushes dependent on production and treatment, Macromolecules 50 (2017) 4715–4724.
[90] O.I. Shchukina, A.V. Zatirakha, A.D. Smolenkov, P.N. Nesterenko, O.A. Shpigun, Anion exchangers with branched functional ion exchange layers of different hydrophilicity for ion chromatography, J. Chromatogr. A 1408 (2015) 78–86.
[91] M. Biesalski, J. Rühe, Scaling laws for the swelling of neutral and charged polymer brushes in good solvents, Macromolecules 35 (2002) 499–507.
[92] Y. Li, Y. Ko, Y. Lin, D. Kiserow, J. Genzer, Enhanced stability of surface-tethered diblock copolymer brushes with a neutral polymer block and a weak polyelectrolyte block: effects of molecular weight and hydrophobicity of the neutral block, Macromolecules 50 (2017) 8580–8587.